Journal of Sound and Vibration (1997) **200**(5), 643–663

NOISE FROM SUPERSONIC COAXIAL JETS, PART 1: MEAN FLOW PREDICTIONS

M. D. Dahl

National Aeronautics and Space Administration, Lewis Research Center, Cleveland, OH 44135, *U.S.A*

AND

P. J. Morris

Department of Aerospace Engineering, The Pennsylvania State University, University Park, PA 16802, *U.S.A.*

(*Received* 5 *February* 1996, *and in final form* 19 *August* 1996)

Recent theories for supersonic jet noise have used an instability wave noise generation model to predict radiated noise. This model requires a known mean flow that has typically been described by simple analytic functions for single jet mean flows. The mean flow of supersonic coaxial jets is not described easily in terms of analytic functions. To provide these profiles at all axial locations, a numerical scheme is developed to calculate the mean flow properties of a coaxial jet. The Reynolds-averaged, compressible, parabolic boundary layer equations are solved using a mixing length turbulence model. Empirical correlations are developed to account for the effects of velocity and temperature ratios and Mach number on the shear layer spreading. Both normal velocity profile and inverted velocity profile coaxial jets are considered. The mixing length model is modified in each case to obtain reasonable results when the two stream jet merges into a single fully developed jet. The mean flow calculations show both good qualitative and quantitative agreement with measurements in single and coaxial jet flows.

1. INTRODUCTION

The current interest in the development of a High Speed Civil Transport that is economically viable and environmentally compatible has renewed research efforts on supersonic jet mixing and noise reduction. Supersonic jets are intense noise generators, and methods must be found to modify the noise generation process to reduce radiated noise levels if a future high speed civilian aircraft is to meet community noise regulations. In a recent review, Seiner and Krejsa [1] discuss the challenge of reducing supersonic jet noise associated with both mixing and shocks while maintaining acceptable propulsion system performance. The goal is to maintain the total thrust and mass flow of the propulsion system at the highest levels while reducing the strength of the noise sources.

One method to modify the noise generated by a supersonic jet is to replace the single stream jet with a dual stream, coaxial jet. Each stream may have a different initial velocity and possibly different initial temperatures. For classification purposes, when the coaxial jet flow has a higher inner stream velocity than an outer stream velocity, it is referred to as a normal velocity profile (NVP) jet, as illustrated in Figure 1(a). If the outer stream velocity is higher than the inner stream velocity, the jet has an inverted velocity profile

0022–460X/97/100643 + 21 $25.00/0/sv960723

(IVP); see Figure 1(b). The temperature of the streams is arbitrary but, for practical propulsion systems, the higher velocity stream typically has the higher temperature.

The analysis to predict the noise generated from supersonic, perfectly expanded jets is based on a theory that instability waves or large scale coherent structures control the development of free jet shear flows. When the instability wave phase velocities exceed the ambient speed of sound, these waves are the dominant source of mixing noise radiated into the downstream arc of the jet. Even when shocks are present in the jet flow, the noise from the jet that radiates into the downstream arc is due primarily to turbulent mixing, whereas the broadband shock associated noise dominates in the upstream arc. Extensive measurements have shown this for single jets [2] and for coaxial jets [3]. The assumption that the jet is perfectly expanded simplifies the analysis and allows us to concentrate on profile shaping as a means to further reduce the mixing noise.

To complete the analysis in the instability wave noise generation model, the equations of motion are decomposed with the assumption that the flow variables are a combination of a mean flow component and a fluctuating component representing the large scale coherent structures. This results in equations that describe the instability waves or large scale structures that are superposed on a known mean flow field. Thus, the mean flow is an input to the instability wave problem and must be determined separately. A complete solution to the instability noise generation model requires that the developing mean flow properties be known at every axial location. In the present paper, we describe an analysis to determine the developing mean flow properties of a compressible coaxial jet. Due to the complex nature of developing NVP and IVP jets with various velocity and temperature conditions, the mean flow has been determined numerically. In related papers, we will

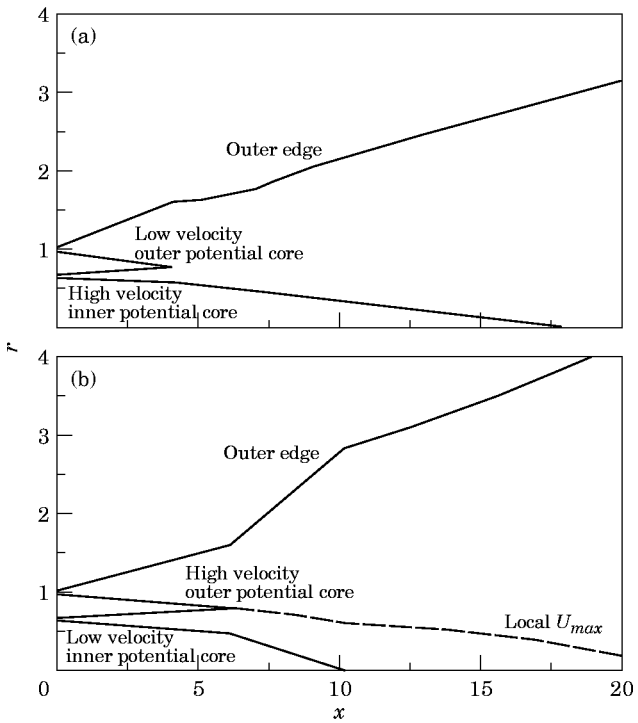

Figure 1. Illustrations of coaxial jet flows: (a) normal velocity profile coaxial jet; (b) inverted velocity profile coaxial jet.

describe the evolution of the instability waves or large scale structures and the noise that they generate and radiate [4, 5].

For the most part, in the past, in calculations of instability waves in a single axisymmetric jet, analytic functions have been used to characterize the mean flow. These analytic functions have been based on results from experimental measurements where data have been correlated by local similarity variables. Examples of this approach include the measurements of: Lau *et al*. [6], whose data were fitted by an error function profile; Cohen and Wygnanski [7], who fitted data with a series of hyperbolic tangent functions, to add corrections to the classical hyperbolic tangent profile; and Morrison and McLaughlin [8], who fitted data by a half-Gaussian profile. Michalke [9] has summarized the use of different analytic functions in the calculation of instability waves. The measured data typically include only velocity profiles, which are sufficient for incompressible instability wave calculations. When compressibility or mean density effects are important, the instability wave calculations require that either the temperature or the density profile be specified. Often, the approximations have been made that allow the Crocco–Busemann relation to be used. This describes the temperature or density profile as a function of the velocity alone [9–11]. Using the methods to be described in this paper, Dahl [12] calculated velocity and density profiles for both subsonic and supersonic jets and compared the results to hyperbolic tangent velocity profiles and the corresponding density profiles from the Crocco-Busemann relation. Good agreement was found for both isothermal and hot jets showing the usefulness of the Crocco–Busemann relation in single jet instability wave calculations. With the mean profile information defined analytically, the mean profile variables and all their derivatives are available at all points in the radial direction for the numerical calculation of instability wave characteristics. Furthermore, these analytic functions may be continued into the complex plane. This allows for the calculation of damped inviscid waves [13]. Thus, the ability to use analytic functions to describe the mean flow simplifies the study of single jet instability waves.

In the case of a coaxial jet, it is not clear how to develop analytic functions to describe the profiles at all axial locations. Tam and Burton [14], in a single supersonic jet case, used a generalized half-Gaussian function to describe the mean velocity at all axial locations. The scaling parameters, the centerline velocity, the core radius, and the half-width of the mixing region, were defined by cubic spline fits to measured data. The density profile was found by keeping the total temperature constant. This approach was possible due to the availability of measured data; however, there is little measured data for coaxial jets, especially with supersonic conditions, that would allow an analytical description to be made at all axial locations, including the merging region of a normal profile and an inverted profile into a single jet. Furthermore, whereas temperature profiles have been measured in a subsonic jet, they are not typically measured in a supersonic jet. Therefore, even though velocity measurements may be available for coaxial jets with supersonic conditions, it is doubtful that the Crocco–Busemann relationship could provide the appropriate temperature profiles for either normal or inverted conditions. Thus, in the present paper the mean profiles for coaxial jets are determined numerically. Morris [15, 16] has calculated instability waves using numerically generated velocity profiles for a single incompressible jet. The significant extension here is the inclusion of compressibility effects and the consideration of both normal and inverted velocity profile coaxial jets.

Techniques to calculate the mean flow properties of coaxial jets numerically have ranged from the use of Reichardt's theory for free turbulence mixing [17–19] to the use of full Navier–Stokes solvers [20]. Early studies primarily modelled subsonic jets and used simple formulations in the turbulence models for the empirically derived constants. More recent studies have used two equation k–ε turbulence models. In all cases, the calculated velocity

profiles resembled measured data with varying degrees of accuracy. However, many of these numerical techniques lack an ease and robustness that is necessary to predict the development of a variety of NVP and IVP jets with a wide variety of operating conditions. To obtain these qualities, a numerical technique based on the approach of Patankar and Spalding [21] has been used. In their work, the development of a turbulent, axisymmetric free jet is assumed to be governed by the Reynolds-averaged, compressible, parabolic boundary layer equations. A turbulence model is required to complete the set of equations. In the next section, we describe the governing boundary layer equations and discuss the basic turbulence model for a single compressible shear layer with different velocity and density ratios. The modifications to the turbulence model are then described for the merging flow in NVP and IVP jets. Next, the numerical formulation is presented. Finally, numerical predictions are made for both single and coaxial jets that compare calculated profiles to measured data and other calculated results for the same jet operating conditions. It should be noted that the goal of this part of the work is the calculation of the mean flow properties of a coaxial jet, either with a normal initial velocity profile or with an inverted initial velocity profile, that expands and merges in a smooth and physically reasonable fashion in the downstream direction. It should be recalled that the resulting predictions of the mean flow development form the basis for an instability wave model of the large scale coherent structures and their noise radiation. Therefore, the absolute accuracy of the calculated mean flows compared to any particular set of measured data is secondary to whether or not the calculated results bear a strong qualitative resemblance to the behavior of coaxial jet flows. However, it will be shown that the predictions, when compared to available measurements, actually show reasonable quantitative agreement.

2. MEAN FLOW DEVELOPMENT

2.1. EQUATIONS FOR COMPRESSIBLE FLOW

The compressible flow of a free jet is governed by the continuity, momentum, energy and state equations. Following the discussion in Anderson *et al*. [22], we assume that the mean flow development of an axisymmetric free jet is governed by the Reynolds-averaged boundary layer equations for compressible flow; since the flow is also assumed to be turbulent. The flow variables are decomposed into a time averaged or mean value part and a fluctuating or turbulent part (e.g., $p = \bar{p} + p'$, where the overbar denotes the time averaged part and the prime denotes the fluctuating part). With the jet static pressure matched to the ambient pressure and the density–velocity and density–enthalpy correlations neglected [23], the equations in axisymmetric co-ordinates reduce to the following:

continuity,

$$\frac{\partial}{\partial x}(r\bar{\rho}\bar{u}) + \frac{\partial}{\partial r}(r\bar{\rho}\tilde{v}) = 0, \tag{1}$$

momentum,

$$\bar{\rho}\bar{u}\frac{\partial \bar{u}}{\partial x} + \bar{\rho}\tilde{v}\frac{\partial \bar{u}}{\partial r} = \frac{1}{r}\frac{\partial}{\partial r}\left[r\left(\mu\frac{\partial \bar{u}}{\partial r} - \bar{\rho}\overline{u'v'}\right)\right], \tag{2}$$

energy,

$$\bar{\rho}\bar{u}\frac{\partial \bar{H}}{\partial x}+\bar{\rho}\tilde{v}\frac{\partial \bar{H}}{\partial r}=\frac{1}{r}\frac{\partial}{\partial r}\left[r\left\{\frac{\mu}{\mathrm{Pr}}\frac{\partial \bar{H}}{\partial r}-\bar{\rho}c_p\overline{v'T'}+\bar{u}\left[\left(1-\frac{1}{\mathrm{Pr}}\right)\mu\frac{\partial \bar{u}}{\partial r}-\bar{\rho}\overline{u'v'}\right]\right\}\right], \tag{3}$$

where $\tilde{v}$ is a mass averaged quantity, defined as

$$\tilde{v}=(1/\bar{\rho})(\bar{\rho}\bar{\mathrm{v}}+\overline{\rho'\mathrm{v}'}). \tag{4}$$

These equations have been non-dimensionalized by the following reference values: spatial co-ordinates by R_1, velocity by U_1, density by ρ_1, pressure by $\rho_1 U_1^2$, enthalpy and c_pT by U_1^2, and viscosity by $R_1\rho_1U_1$. The subscript 1 is used to indicate jet exit conditions for a single jet or for the inner stream of a coaxial jet.

We assume a perfect gas. Thus, the equation of state is

$$\bar{p}=\bar{\rho}R_g\bar{T}, \tag{5}$$

where R_g is the gas constant. Also, the laminar viscosity is related to the mean temperature according to Sutherland's Law:

$$\mu=\mu_0\left(\frac{\bar{T}}{T_0}\right)^{3/2}\frac{T_0+S_0}{\bar{T}+S_0}. \tag{6}$$

S_0 is 110·3 and μ_0 is the viscosity at the reference temperature T_0 of 273 K.

2.2. TURBULENCE MODEL

In equations (2) and (3), the Reynolds stress term $-\bar{\rho}\overline{u'v'}$ and the Reynolds heat flux term $-\bar{\rho}c_p\overline{v'T'}$ are undefined. These terms must be modelled in order to solve the system of equations. In anticipation of the difficulties in the definition of a turbulence model that would work for a supersonic coaxial jet with both normal or inverted initial velocity profiles and streams of different temperature (an example of the difficulties in turbulence modelling for single stream supersonic jets is found in Dash [24]) it was decided to use the most basic model; namely, the mixing length model for the turbulence closure. Any turbulence model chosen for these calculations would require modification and calibration to obtain reasonable results for both normal and inverted profile coaxial jets. The mixing length model represents the turbulent stress from which an effective viscosity is defined. Through the use of a turbulent Prandtl number to relate eddy diffusivities for heat and momentum, an effective Prandtl number may be calculated from the effective viscosity.

In the mixing length model, the Reynolds stress term is written as [10, 22]

$$-\bar{\rho}\overline{u'v'}=\mu_{\mathrm{T}}\frac{\partial \bar{u}}{\partial r} \tag{7}$$

and the heat flux term as

$$-\bar{\rho}c_p\overline{v'T'}=\frac{c_p\mu_{\mathrm{T}}}{\mathrm{Pr}_{\mathrm{T}}}\frac{\partial \bar{T}}{\partial r}. \tag{8}$$

The turbulent Prandtl number Pr_{T} has essentially a constant value for free jet calculations [10, 22, 25, 26]. The mixing length model is embodied in the turbulent viscosity,

$$\mu_{\mathrm{T}}=\bar{\rho}(C_1C_2l)^2|\partial\bar{u}/\partial r|, \tag{9}$$

where l is a characteristic length scale, and C_1 and C_2 are mixing length constants; however, for this model, they are taken to be functions of the flow conditions.

It is known that the growth of a shear layer depends on the flow conditions at the shear layer edges with the velocities and densities of the two streams being of primary interest [10, 25, 27, 28]. This dependence occurs whether the flow is compressible or incompressible. In an attempt to separate out purely compressible effects, Papamoschou and Roshko [28] and others have normalized the compressible shear layer growth rate by an incompressible growth rate value at the same edge conditions. This followed the earlier work of Brown and Roshko [27], that showed the effects of different velocity and density edge conditions on shear layer growth for incompressible flows. Thus, in order to incorporate these effects into the mixing length model, to obtain the proper shear layer growth, two factors have been developed that depend on the flow conditions; one for incompressible conditions and the other for compressibility effects.

The factor C_1 is the incompressible part of the mixing length constant. It depends on the velocity ratio U_2/U_1 and the density ratio ρ_2/ρ_1 between the two streams on either side of the shear layer, where U_1 and ρ_1 are the mean velocity and density of the inner stream and U_2 and ρ_2 are the mean velocity and density of the outer stream. Correlations for the expected vorticity thickness growth rate have been developed by many investigators from experimental evidence. Thus, given that we know the vorticity thickness growth rate for a fixed velocity ratio and a fixed density ratio, we have adjusted C_1 ($C_2 = 1$) until the calculated initial vorticity thickness growth rate of a single jet agrees with the correlated value. Continuing this process for a range of velocity and density ratio values results in a series of calibration curves for C_1.

C_2 is the compressible part of the mixing length definition. Its purpose is to decrease the growth of the shear layer as compressibility effects become important. It depends on a Mach number in a relative frame of reference convecting with the real phase speed of a growing disturbance in the shear layer. This convective Mach number depends on the velocity ratio, on the density ratio, and on the Mach number of one of the streams. The convective Mach number has been used to correlate normalized measured growth rates of compressible shear layers. We have developed an equation that fits this data in order to predict shear layer growth rates for given flow conditions. Thus, we have proceeded to determine C_2 given that C_1 is allowed to take on its previously calibrated value for the given velocity and density ratios. C_2 is adjusted until the calculated initial vorticity thickness growth rate agrees with the predicted value. For this case, a single calibration curve has been generated. Further details on the evaluation of C_1 and C_2 are given in Appendix A.

There are several choices that may be made for the characteristic length scale for a jet shear layer. Since the flow is turbulent and the motion is dominated by large structures or instability waves, an appropriate characteristic length scale would be [27, 29]

$$l = \Delta\bar{u}/|\partial\bar{u}/\partial r|_{max}, \tag{10}$$

where $\Delta\bar{u}$ is the velocity difference across the shear layer. Defined in this way, l can be interpreted as a vorticity thickness. If necessary, it can be related to other length scales if an appropriate functional shape for the velocity profile is chosen. For example, $l = 0{\cdot}978 l_w$ where l_w is defined as the shear layer width from the location at which $(\bar{u} - \bar{u}_2)/\Delta\bar{u} = 0{\cdot}9$ to the location at which $(\bar{u} - \bar{u}_2)/\Delta\bar{u} = 0{\cdot}1$; $\bar{u}$ is described by an error function, and $\bar{u}_2$ is the normalized outer stream velocity.

2.3. COAXIAL JET MIXING LENGTH MODEL

Initially, a coaxial jet, either with an initial normal velocity profile or an inverted velocity profile, has two distinct shear layers with uniform flow conditions at both edges of both shear layers. As a result, the mixing length model, equation (9), gives separate constant values C_1, C_2, and l for each layer. The values of C_1 and C_2 depend on the velocity ratio,

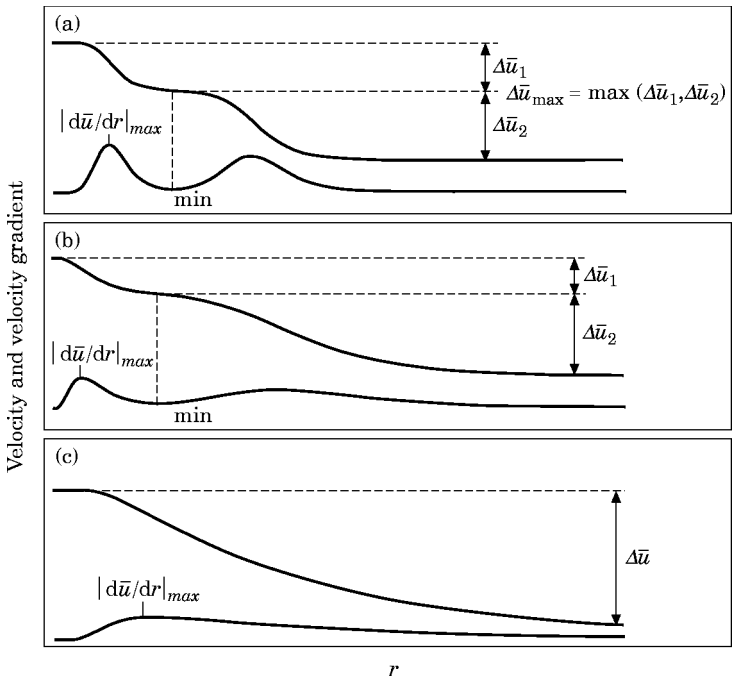

Figure 2. Definitions of the merging normal velocity profile mixing length model factors: (a) initial merging profile; (b) advanced merging profile; (c) fully merged profile.

the density ratio and the convective Mach number determined from the separate edge conditions. The characteristic length l is determined for each shear layer from equation (10). The turbulent viscosity μ_T is then calculated across the coaxial jet using local values of $\bar{\rho}$ and $|\partial\bar{u}/\partial r|$. The separate shear layers have different constants (C_1, C_2, l) so that, at some point between the two shear layers, the μ_T profile must switch from one set of constants to the other. As a result, an abrupt change in the μ_T profile occurs that is not desirable numerically. Initially, $|\partial\bar{u}/\partial r|$ is near zero between the two shear layers and the effect of the abrupt change is negligible. As the calculations progress downstream, $|\partial\bar{u}/\partial r|$ between the two shear layers increases and the jump in μ_T is appreciable. To overcome this problem, a hyperbolic tangent function is used to transpose from one set of constants to the other. This works until the outer jet core is about to disappear and the shear layers are about to merge. At that point, the mixing length model must be altered and the normal and the inverted velocity profile cases are treated separately.

2.3.1. *Normal velocity profile mixing length model*

The normal velocity profile mixing length model has been developed by observations of the behavior of the $\bar{u}$ and $\partial\bar{u}/\partial r$ profiles as the shear layers merge and by a comparison of calculations to measured data taken from Lau [30]. The merging shear layer profile contains a local minimum in $|\partial\bar{u}/\partial r|$ that disappears as the shear layer merges fully into a single jet; see Figure 2. This local minimum is used as a point to separate the two merging shear layers. A single characteristic length for the merging shear layers is defined as

$$l = \Delta\bar{u}_{max}/|\partial\bar{u}/\partial r|_{max}, \tag{11}$$

where $\Delta\bar{u}_{max}$ is the larger $\Delta\bar{u}$ between the two values determined by using the separation point. The values of C_1 and C_2 are also determined from the edge conditions that give

$\Delta\bar{u}_{max}$. The maximum gradient $|\partial\bar{u}/\partial r|_{max}$ is the largest value of $|\partial\bar{u}/\partial r|$ that occurs in the merging profile. This method for the determination of C_1, C_2 and l for a merging normal profile has the advantage that, as the flow transposes into a single jet profile, the C_1, C_2, and l values transition into the appropriate form for a single jet.

2.3.2. *Inverted velocity profile mixing length model*

When an inverted profile starts to merge, a local maximum occurs in the velocity profile yielding $\partial\bar{u}/\partial r = 0$; see Figure 3(a). This point is used to identify the separation point between the two shear layers. As long as the inner core exists, the two merging shear layers are treated separately but their constants are added as follows:

$$(C_1C_2l)_{total} = (C_1C_2l)_{inner} + (C_1C_2l)_{outer}. \tag{12}$$

This increases μ_T across the profile to mimic the increased turbulent action as the inverted profile starts to merge. When the inner core ends, equation (12) is no longer used and it is assumed that the mixing process in the outer shear layer dominates the flow, so that, $(C_1C_2l)_{total} = (C_1C_2l)_{outer}$; see Figure 3(b). As with the normal profile, this later usage of C_1, C_2, and l transitions into the proper usage for a single jet downstream. It should be noted that the mixing length model gives $\mu_T = 0$ at the local maximum, which is unrealistic. The simple solution taken here is to smooth the $|\partial\bar{u}/\partial r|$ profile, and hence smooth μ_T [12].

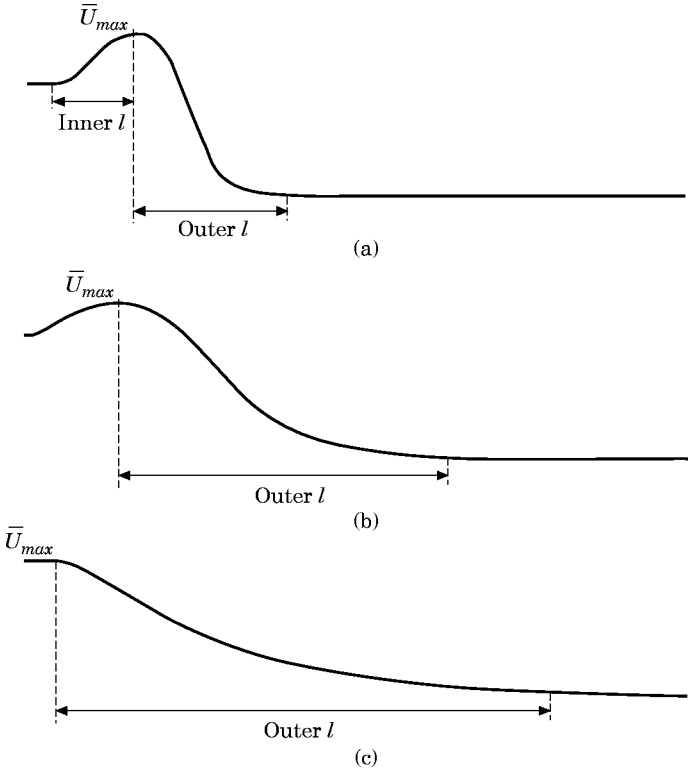

Figure 3. Definitions of the merging inverted velocity profile mixing length model factors: (a) initial merging profile; (b) advanced merging profile, no inner stream potential core; (c) fully merged profile.

2.4. NUMERICAL FORMULATION

Many numerical techniques are available for the solution of the boundary layer equations. Any of these could have provided adequate mean flow results; but our criterion for mean flow calculations dictated that the mean flow results be sufficiently resolved in order to be used for instability wave calculations. Furthermore, we wished to avoid any numerical calculation of $\tilde{v}$. Hence, initially, we followed the stream function approach used by Patankar and Spalding [21] and Crawford and Kays [26].

The equations of motion are transformed to stream function co-ordinates using

$$r\bar{\rho}\bar{u} = \partial\Psi/\partial r, \qquad r\bar{\rho}\bar{v} = -\partial\Psi/\partial x. \tag{13}$$

These equations ensure that the continuity equation (1) is satisfied. After substitution of equations (7) and (8) into equations (2) and (3) and with the use of the definition for total enthalpy $\bar{H} = c_p\bar{T} + \bar{u}^2/2$, followed by a transformation from (x, r) co-ordinates to (x, Ψ) co-ordinates, we obtain for momentum and energy:

$$\frac{\partial\bar{u}}{\partial x} = \frac{\partial}{\partial\Psi}\left[r^2\bar{\rho}\bar{u}\mu_{eff}\frac{\partial\bar{u}}{\partial\Psi}\right], \tag{14}$$

$$\frac{\partial\bar{H}}{\partial x} = \frac{\partial}{\partial\Psi}\left[r^2\bar{\rho}\bar{u}\frac{\mu_{eff}}{\mathrm{Pr}_{eff}}\frac{\partial\bar{H}}{\partial\Psi}\right] + \frac{\partial}{\partial\Psi}\left[r^2\bar{\rho}\bar{u}^2\left(\mu_{eff} - \frac{\mu_{eff}}{\mathrm{Pr}_{eff}}\right)\frac{\partial\bar{u}}{\partial\Psi}\right], \tag{15}$$

where

$$\mu_{eff} = \mu + \mu_{\mathrm{T}}, \qquad \mathrm{Pr}_{eff} = \frac{1 + \mu_{\mathrm{T}}/\mu}{1/\mathrm{Pr} + \mu_{\mathrm{T}}/\mathrm{Pr}_{\mathrm{T}}\mu} \tag{16, 17}$$

These equations can be differenced in a variety of ways: explicitly [31], implicitly on an evenly spaced Ψ-grid [32], or transformed to a normalized Ψ-grid and implicitly differenced as in Patankar and Spalding [21]. Each of these numerical methods have been found to have problems. The explicit DuFort–Frankel method [31] has stability problems; the implicit Crank–Nicolson method using an evenly spaced Ψ-grid [32] does not provide sufficient resolution at the outer, low speed edges of the jet; and Patankar and Spalding's method [21] has difficulties with entrainment boundary conditions at the outer edge. Each of these problems have been overcome by using fully implicit differencing and what is considered to be a natural grid stretching and a natural outer boundary entrainment. By choosing a fully implicit method, the numerical problem is inherently stable. The problem of grid resolution is overcome by the use of an evenly spaced r-grid. The outer boundary condition is discussed later.

The choice of an evenly spaced r-grid results in an unevenly spaced Ψ-grid. In essence, the Ψ-grid is stretched, but in a manner that is natural to the Ψ-grid, with more grid points at the outer edge where a finer grid spacing is desired. From equation (13),

$$\mathrm{d}\Psi = r\bar{\rho}\bar{u}\,\mathrm{d}r. \tag{18}$$

Integration of equation (18) across one grid spacing we obtain

$$\Delta\Psi_k = \Psi_k - \Psi_{k-1} = \tfrac{1}{2}[(r\bar{\rho}\bar{u})_k + (r\bar{\rho}\bar{u})_{k-1}]\Delta r \tag{19}$$

after using the trapezoidal rule. One consequence of equation (19) is that $\bar{u}$ cannot be zero outside the jet or $\Delta\Psi$ would go to zero. To get close to quiescent outer conditions, the free stream velocity is set to 1% of the initial highest velocity.

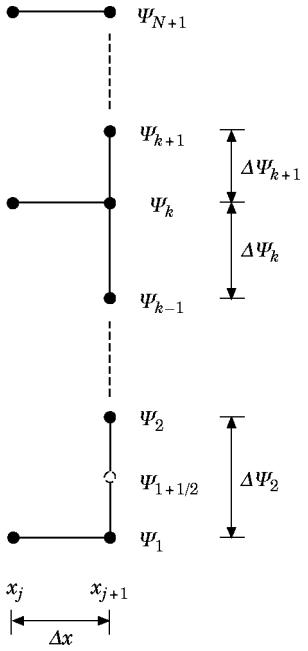

Figure 4. The stream function grid for mean flow calculations.

Writing equation (14) as

$$\frac{\partial \bar{u}}{\partial x} = \frac{\partial}{\partial \Psi}\left[A \frac{\partial \bar{u}}{\partial \Psi} \right], \tag{20}$$

where

$$A = r^2 \bar{\rho} \bar{u} \mu_{eff}, \tag{21}$$

we implicitly difference this momentum equation, using the grid shown in Figure 4, as follows:

$$\frac{\bar{u}_{j+1,k} - \bar{u}_{j,k}}{\Delta x} = \left\{ \frac{2}{\Delta\Psi_{k+1} + \Delta\Psi_k} \left[A_{k+1/2} \frac{\bar{u}_{k+1} - \bar{u}_k}{\Delta\Psi_{k+1}} - A_{k-1/2} \frac{\bar{u}_k - \bar{u}_{k-1}}{\Delta\Psi_k} \right] \right\}_{j+1}. \tag{22}$$

The coefficient A is the average of adjacent grid values

$$A_{k+1/2} = \tfrac{1}{2}(A_k + A_{k+1}). \tag{23}$$

Collecting terms, equation (22) may be arranged into tridiagonal form

$$\{ -\Delta_k^- A_{k-1/2} \bar{u}_{k-1} + (1 + \Delta_k^+ A_{k+1/2} + \Delta_k^- A_{k-1/2}) \bar{u}_k - \Delta_k^+ A_{k+1/2} \bar{u}_{k+1} \}_{j+1} = \bar{u}_{j,k}, \tag{24}$$

where

$$\Delta_k^- = \frac{2\Delta x}{(\Delta\Psi_{k+1} + \Delta\Psi_k)\Delta\Psi_k}, \qquad \Delta_k^+ = \frac{2\Delta x}{(\Delta\Psi_{k+1} + \Delta\Psi_k)\Delta\Psi_{k+1}}. \tag{25, 26}$$

Equation (15) is differenced in the same manner. The resulting tridiagonal equation is

$$\{-\Delta_k^- D_{k-1/2}\bar{u}_{k-1} - \Delta_k^- B_{k-1/2}\bar{H}_{k-1} + (\Delta_k^+ D_{k+1/2} + \Delta_k^- D_{k-1/2})\bar{u}_k + (1 + \Delta_k^+ B_{k+1/2} + \Delta_k^- B_{k-1/2})\bar{H}_k - \Delta_k^+ D_{k+1/2}\bar{u}_{k+1} - \Delta_k^+ B_{k+1/2}\bar{H}_{k+1}\}_{j+1} = \bar{H}_{j,k}, \quad (27)$$

where

$$B = r^2\bar{\rho}\bar{u}\frac{\mu_{eff}}{\mathrm{Pr}_{eff}}, \qquad D = r^2\bar{\rho}\bar{u}^2\left(\mu_{eff} - \frac{\mu_{eff}}{\mathrm{Pr}_{eff}}\right). \quad (28, 29)$$

2.4.1. *Boundary conditions*

Since the problem is axisymmetric, a symmetry boundary condition is enforced at $r = 0$, $k = 1$; that is,

$$\partial\bar{u}/\partial\Psi = \partial\bar{H}/\partial\Psi = 0. \quad (30)$$

The right side of equation (20) is differenced using half the grid spacing at the edge (see Figure 4):

$$\frac{\bar{u}_{j+1,1} - \bar{u}_{j,1}}{\Delta x} = \frac{1}{\Delta\Psi_2/2} = \left\{\left[A\frac{\partial\bar{u}}{\partial\Psi}\right]_{j+1,1+1/2} - \left[A\frac{\partial\bar{u}}{\partial\Psi}\right]_{j+1,1}\right\}. \quad (31)$$

From the boundary condition (30), the $(j + 1, 1)$ term on the right side is zero. The final tridiagonal form is

$$\left\{\left(1 + \frac{2\Delta x}{\Delta\Psi_2^2}A_{1+1/2}\right)\bar{u}_1 - \frac{2\Delta x}{\Delta\Psi_2^2}A_{1+1/2}\bar{u}_2\right\}_{j+1} = \bar{u}_{j,1}. \quad (32)$$

Similarly, for the energy equation we obtain

$$\left\{\frac{2\Delta x}{\Delta\Psi_2^2}D_{1+1/2}\bar{u}_1 + \left(1 + \frac{2\Delta x}{\Delta\Psi_2^2}B_{1+1/2}\right)\bar{H}_1 - \frac{2\Delta x}{\Delta\Psi_2^2}D_{1+1/2}\bar{u}_2 - \frac{2\Delta x}{\Delta\Psi_2^2}B_{1+1/2}\bar{H}_2\right\}_{j+1} = \bar{H}_{j,1}. \quad (33)$$

The outer boundary condition is simply that the $\bar{u}$ and $\bar{H}$ values equal the free stream conditions; that is,

$$\bar{u}_{j+1,N+1} = \bar{u}_{j,N+1} = \bar{u}_\infty, \qquad \bar{H}_{j+1,N+1} = \bar{H}_{j,N+1} = \bar{H}_\infty. \quad (34)$$

This also may be viewed as saying that derivatives in the x-direction are zero at the outer edge. The consequence of this type of boundary condition is that the flow, expanding outward due to diffusion, must never reach the outer grid boundary or the calculations will be in error. The method by which this difficulty is overcome is discussed in the next section.

2.4.2. *Numerical method of solution*

Equations (24), (27), (32), (33) and (34), create a 2×2 block tridiagonal system for $k = 1$ to $N + 1$, where N is the number of grid spacings. The system can be solved by standard block tridiagonal routines [22]. The coefficient matrices of the block tridiagonal system are unknown at the $j + 1$ location since they are functions of the unknowns, $\bar{u}_{j+1,k}$ and $\bar{H}_{j+1,k}$. Consequently, iterations must be made to complete the solution for each axial step. The procedure is as follows.

1. Guess $\bar{u}_{j+1,k}$ and $\bar{H}_{j+1,k}$. If $j = 1$, then use the initial conditions:

$$\bar{u}_{2,k} = \bar{u}_{1,k}, \qquad \bar{H}_{2,k} = \bar{H}_{1,k}.$$

For $j > 1$, we can extrapolate from previous solutions:

$$\bar{u}_{j+1,k} = 2\bar{u}_{j,k} - \bar{u}_{j-1,k}, \qquad \bar{H}_{j+1,k} = 2\bar{H}_{j,k} - \bar{H}_{j-1,k}.$$

2. Solve for $j + 1$ values of $\bar{\rho}$, u_{eff} and Pr_{eff}.
3. Calculate $\Delta\Psi_{j+1,k}$ grid using equation (19).
4. Solve the block tridiagonal system for new values of $\bar{u}_{j+1,k}$ and $\bar{H}_{j+1,k}$. Also, new values of $\bar{\rho}$, μ_{eff} and Pr_{eff} are calculated.
5. If the difference between the new solution and the previous solution is smaller than some convergence criterion, then the axial step is completed. Otherwise, the iteration process continues at step 3.

To ensure, as mentioned previously, that the outer boundary condition is not compromised by the expanding flow, the grid must be large enough in the radial direction to encompass the flow. Rather than making the grid so large that the flow is encompassed at all axial locations, the outer edge of the initial grid is much closer to the outer edge of the jet, typically the grid ends at twice the outer radius of the initial jet. As the flow expands downstream, the outer edge of the jet flow is tracked until it is within some arbitrary distance from the outer edge of the grid; at which time, more grid points are added to the solution. All of the variables at the new grid points take on the free stream values that are assumed to always exist outside the grid. As the shear layer of the jet expands, it becomes possible to increase the Δr-grid spacing since less grid points are necessary to define the shear layer. Thus, we do not simply continue to add grid points as the flow expands but, from time to time, we reduce the number of grid points by increasing the grid spacing. Actually, it is best to simply double the grid spacing so that the extrapolated guesses for the new variables occur along constant grid lines in the x-direction. Thus, no interpolation is necessary.

2.4.3. *Numerical accuracy*

The numerical scheme for the governing parabolic equations, equation (22) for example, is first order accurate in both Δx and $\Delta\Psi$. The latter accuracy is due to the uneven spacing in the Ψ-grid. Since the mean flow results are used in the stability calculations, it is found there that to obtain converged stability results a finely spaced r-grid is necessary for the calculation of the derivatives of the mean flow variables. Using a fine r-grid results, through equation (19), in a fine, but unevenly spaced Ψ-grid. An example to illustrate the convergence of the mean flow calculations using the mixing length turbulence model is shown in Figure 5 for three different grid spacings. The calculated shear layer half-width b and the vorticity thickness δ are shown for the shear layer of a single jet under both incompressible and compressible conditions. The half-width shows the ability of the code to find the defined edges of the shear layer in order to calculate the half-width and vorticity thickness shows its ability to calculate accurately the maximum derivative of the mean velocity profile. For the range of grid spacings shown, the mean flow results are independent of the grid spacing.

3. NUMERICAL PREDICTION

3.1. SINGLE JET CALCULATIONS

The numerical predictions are compared in Figure 6 to data taken form Zaman [33] for a subsonic, $M = 0{\cdot}5$ axisymmetric jet. The axial variation of the centerline velocity is

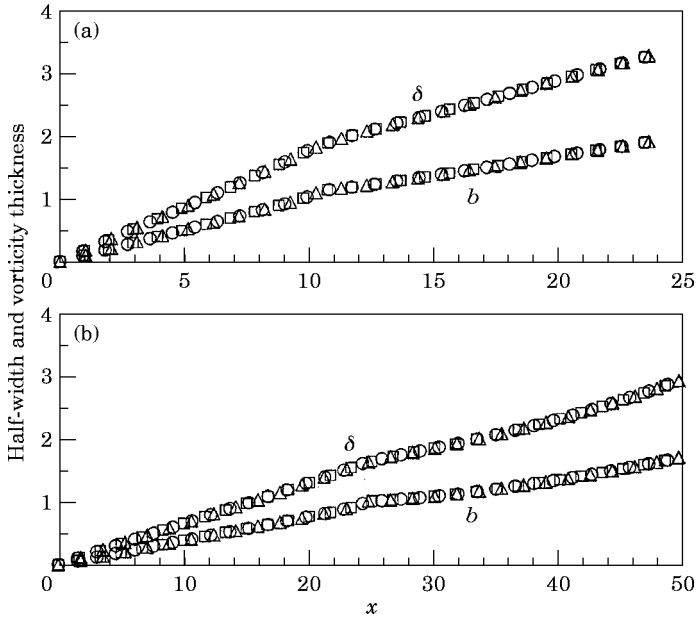

Figure 5. Results for the single jet spreading parameters vorticity thickness δ and jet half-width b at three different radial grid spacings: ○, $\Delta r = 0{\cdot}004$, $N = 500$; □, $\Delta r = 0{\cdot}002$, $N = 1000$; △, $\Delta r = 0{\cdot}001$, $N = 2000$. (a) Incompressible single jet parameters; (b) compressible single jet parameters.

shown in Figure 6(a). The calculations show good agreement with the data and to an equation for centerline velocity from Witze [34], based on a correlation of many different jet measurements. In Figure 6(b) are shown the growth of the jet half-velocity width and the ratio of the jet half-velocity width to momentum thickness. The calculations underpredict the spread of the jet as defined by the half-velocity width.

Results for higher speed jets are shown in Figure 7. For the $M = 1{\cdot}37$ jet, the centerline velocity data are taken from Lau *et al*. [6] (Figure 7(a)) and the half-velocity point data

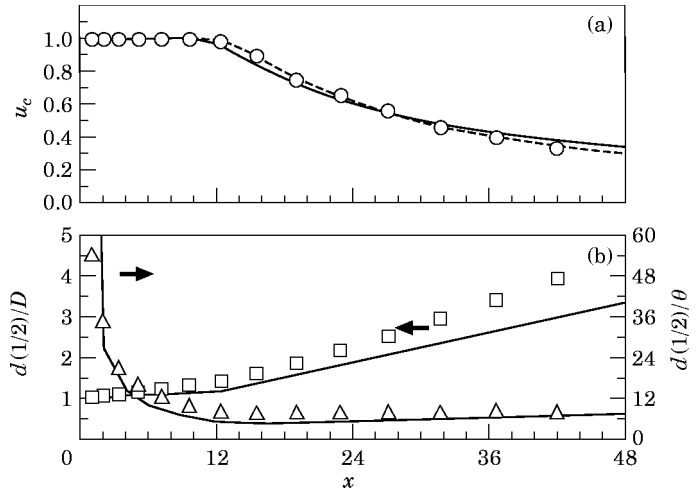

Figure 6. A comparison of subsonic single jet calculations ($M = 0{\cdot}5$) to measured data [33]. (a) Centerline velocity: ——, calculated; ○, data; – – –, Witze [34] centerline; (b) jet half-velocity width/jet exit diameter, □ (left scale); jet half-velocity width/momentum thickness, △ (right scale); ——, calculated. Operating conditions: $U_1 = 172{\cdot}5$ m/s, $T_1 = 295{\cdot}4$ K, $R_1 = 1{\cdot}27$ cm.

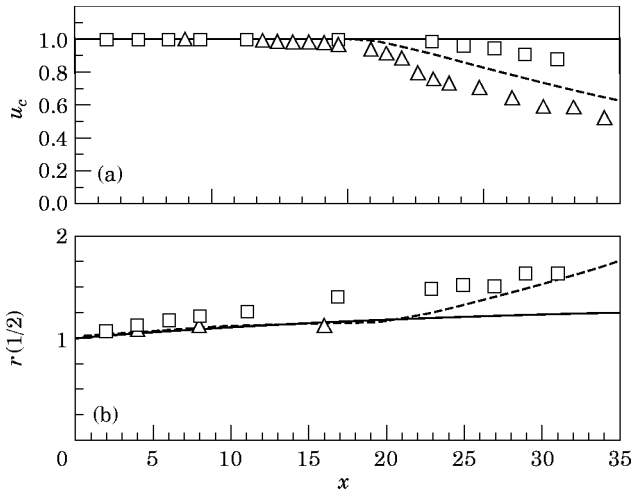

Figure 7. A comparison of subsonic single jet calculations to measured data. (a) centerline velocity: (b) jet half-velocity point. Operating conditions: $M = 2{\cdot}22$, $U_1 = 538$ m/s, $T_1 = 147$ K, $R_1 = 1{\cdot}28$ cm; ——, calculated; □, data [36]; $M = 1{\cdot}37$, $U_1 = 472$ m/s, $T_1 = 295{\cdot}4$ K, $R_1 = 2{\cdot}55$ cm; — — —, calculated; △, data [6, 35].

is from Lau [35] (Figure 7(b)). The calculated core region spreads at the measured rate, although the measured core length is slightly shorter than predicted. For the $M = 2{\cdot}22$ jet, the comparisons for both the centerline velocity and the jet half-velocity point are made with data from Eggers [36]. Again, the calculations underpredict the measured spreading of the jet. These results show the inaccuracies that exist in trying to model the effects of compressibility in our mean flow calculations. The calculated spreading rate of a compressible jet is determined by the compressible calibration equation (A3) given in Appendix A. The measured spreading rate data are scattered around this correlation and the predictions reflect these discrepancies. Any measured jet spreading rate data that are larger than that predicted by the calibration equation will have calculated spreading rates that are less than the measured spreading rates. This is reflected in the comparison between the calculated jet half-velocity point and the data measured by Eggers. Since the experimental jet spreading rate is higher than that predicted by the calibration equation, the measured jet half-velocity point moves outward faster downstream than predicted (Figure 7(b)). Experimental jets that have spreading rates much closer to the calibration curve (e.g., the measured Lau data) have better agreement between the calculated and the measured jet half-velocity points. As with many other attempts at turbulence modelling, the results are only as good as the calibration and it is difficult to apply the same model to experiments for a wide range of operating conditions in many different facilities. Also, the turbulence model is calibrated to match growth rates in the initial core region of a jet, the region of most importance to growing instabilities. In the downstream region, the jet is a thick axisymmetric shear layer and the current turbulence model, based on thin shear layer results, provides less representative growth rates.

A final comparison is made for a single jet in a moving stream. These results are important to the subsequent consideration of coaxial jets on the effect of Mach number and the effect of velocity ratio on jet spreading characteristics. The effect of the velocity ratio on the centerline velocity is shown in Figure 8(a). The calculated results show that the turbulence model gives a decrease in jet spreading and an increase in the potential core length as the velocty ratio increases from 0·096 to 0·497. This agrees with the results

measured by Morris [29] for the effects of velocity ratio on centerline velocity. The Mach number effect at a velocity ratio of about 0·1 is shown in Figure 8(b). Again, the calculated results behave in the same manner as the measured data as the Mach number increases from 0·47 to 1·67. Hence, the turbulence model allows for the calculated jet behavior to mimic the expected jet behavior for a compressible jet in a co-flowing stream.

3.2. COAXIAL JET CALCULATIONS

With the single shear layer turbulence model tested on both subsonic and supersonic jets with and without a co-flowing stream, we now add an outer jet flow to create a coaxial jet with two shear layers. Both NVP and IVP jet examples are considered. A comparison of calculated velocity profiles for a NVP jet to measured data [30] at four axial locations is shown in Figure 9. Initially, the agreement is very good. The outer shear layer is spreading faster than the inner shear layer, as expected from the results in Figure 8 for a jet in a co-flowing stream. Downstream, the calculated jet centerline velocity begins to decay sooner than the measured data. This again reflects the differences between the correlation for the spreading rate and the measured values for this set of data. However, in essence, the calculations produce a reasonable representation of the merging jet for an initial normal velocity profile.

Next, the inverted velocity profile data from von Glahn *et al*. [37] are used for comparison with calculations. Velocity profiles measured at five axial locations are shown in Figure 10. The IVP predictions show similar velocity profiles as the two shear layers spread and merge downstream. The other calculated results shown in the figure are from Georgiadis and Yoder [20]. Their results are indicative of the problems encountered when using Navier–Stokes solvers with k–ϵ turbulence models. The initial profiles are not smooth and the spreading of the shear layer downstream is greatly underpredicted.

A final comparison with IVP jet data is shown for both velocity and temperature profiles in Figures 11 and 12: the data are from Tanna *et al*. [38]. In this case, the outer stream is much thinner than in the previous example causing the two shear layers to mix sooner.

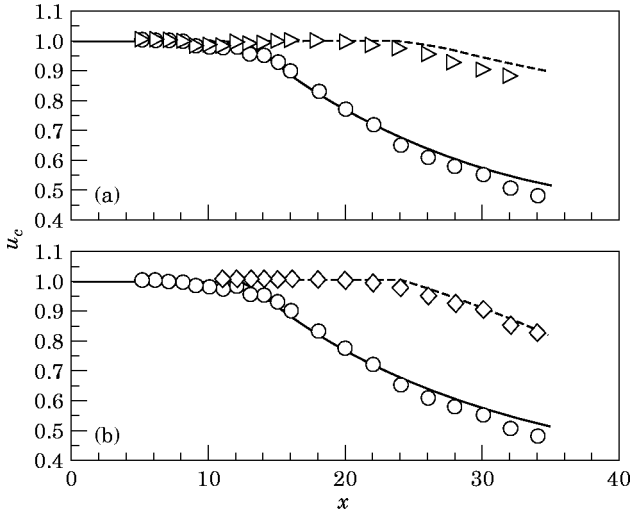

Figure 8. A comparison of single jet in moving stream calculations to measured data [29]. (a) Centerline velocity variations with external flow: ——, calculated, $M = 0{\cdot}47$, $U_2/U_1 = 0{\cdot}096$; ○, data; — — —, calculated, $M = 0{\cdot}47$, $U_2/U_1 = 0{\cdot}497$; ▷, data. (b) Centerline velocity variations with Mach number: ——, calculated, $M = 0{\cdot}47$, $U_2/U_1 = 0{\cdot}096$; ○, data; — — —, calculated, $M = 1{\cdot}67$, $U_2/U_1 = 0{\cdot}098$; ◇, data. Operating conditions $R_1 = 2{\cdot}54$ cm; $M = 0{\cdot}47$, $U_1 = 158$ m/s, $T_1 = 283$ K; $M = 1{\cdot}67$, $U_1 = 461$ m/s, $T_1 = 190$ K.

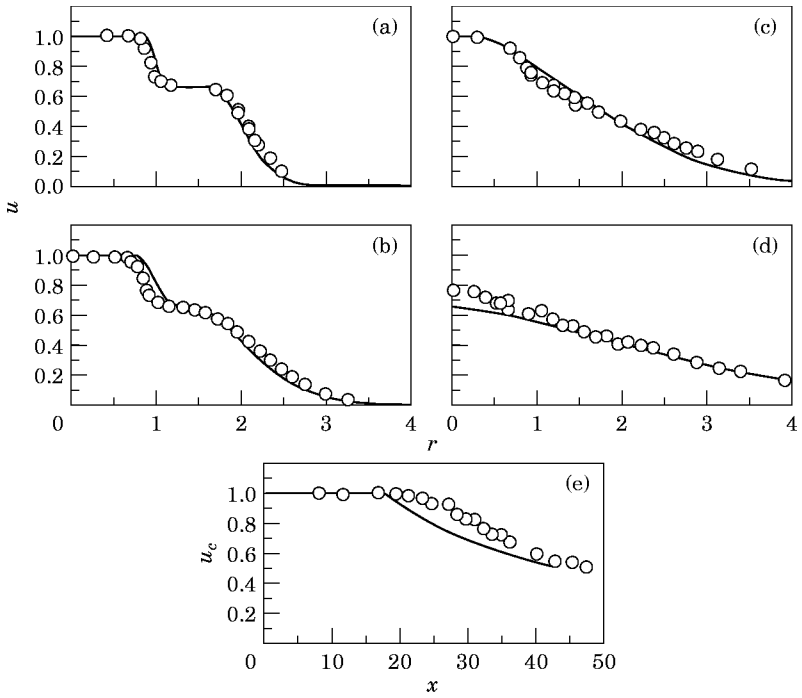

Figure 9. A comparison of normal velocity profile jet calculations to measured data [30]: ——, calculated; ○, data. Radial velocity profiles: (a) $x = 4$; (b) $x = 8$; (c) $x = 16$; (d) $x = 32$. (e) Centerline velocity. Operating conditions: $U_1 = 411$ m/s, $T_1 = 657$ K, $R_1 = 1{\cdot}96$ cm; $U_2 = 274$ m/s, $T_2 = 292$ K, $R_2 = 3{\cdot}91$ cm.

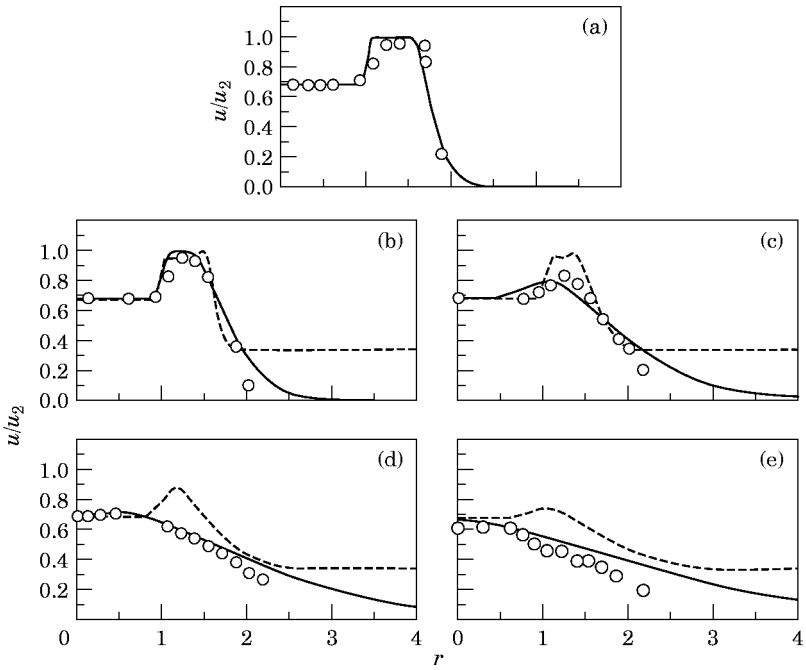

Figure 10. A comparison of inverted velocity profile jet calculations to measured data [37]: ——, calculated; ○, data; — — —, calculated in reference [20]. Radial velocity profiles: (a) $x = 2$; (b) $x = 4$; (c) $x = 8$; (d) $x = 16$. (e) $x = 26$. Operating conditions: $U_1 = 314$ m/s, $T_1 = 248$ K, $R_1 = 5{\cdot}03$ cm; $U_2 = 459$ m/s, $T_2 = 1029$ K, $R_2 = 8{\cdot}80$ cm.

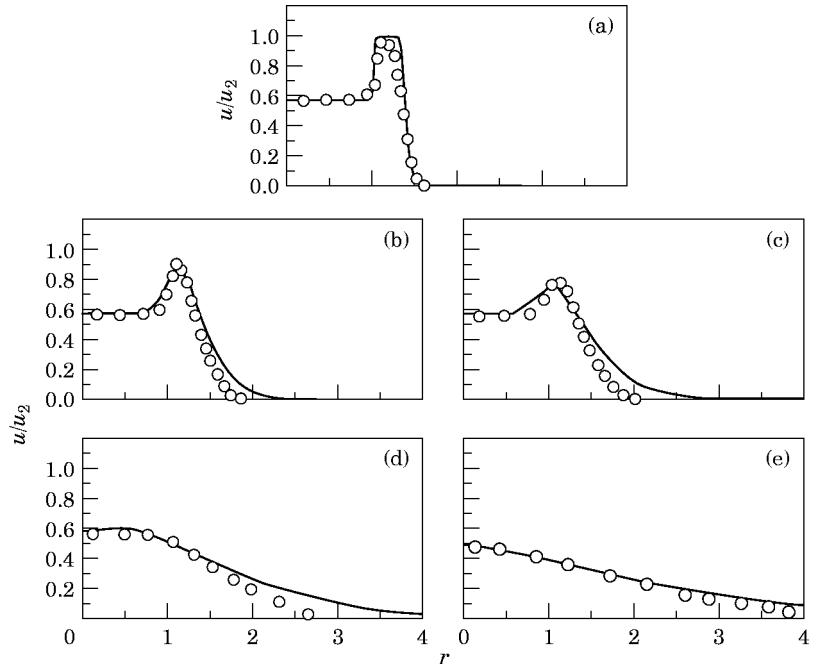

Figure 11. A comparison of inverted velocity profile jet calculations to measured data [38]: ——, calculated; ○, data. Radial velocity profiles: (a) $x = 0{\cdot}38$; (b) $x = 2{\cdot}7$; (c) $x = 3{\cdot}8$; (d) $x = 11{\cdot}5$; (e) x = 23·0. Operating conditions: $U_1 = 273$ m/s, $T_1 = 434$ K, $R_1 = 2{\cdot}61$ cm; $U_2 = 477$ m/s, $T_2 = 758$ K, $R_2 = 3{\cdot}57$ cm.

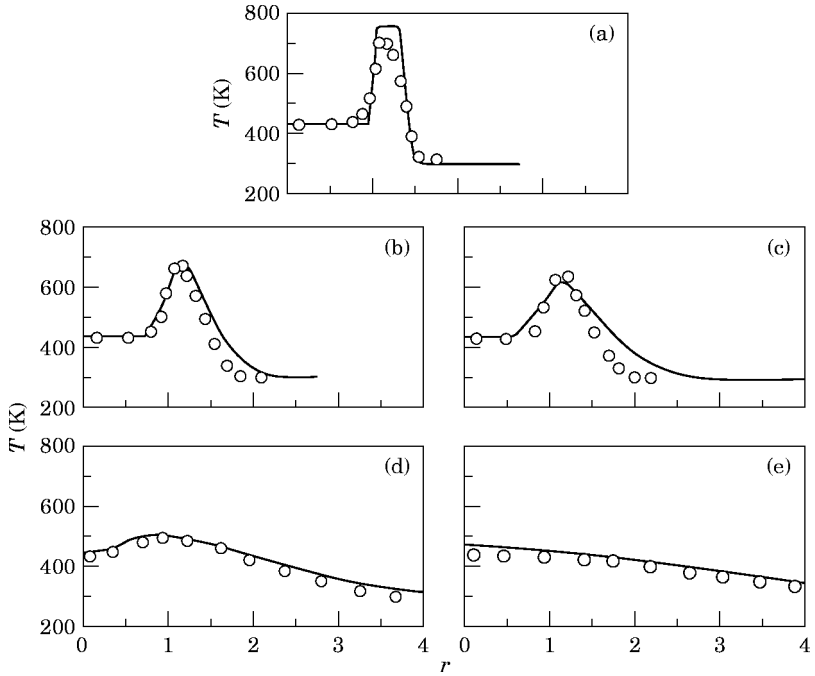

Figure 12. A comparison of inverted velocity profile jet temperature calculations to measured data [38]. See Figure 11 for legend and operating conditions.

Both good qualitative and quantitative agreement is seen for the velocity and temperature profiles. Thus, the present calculations are capable of producing a reasonable merging jet with an initial inverted velocity profile.

4. SUMMARY

Much of the thoretical work on the stability of free shear flows relies on the analytical definition of the mean flow in order to solve for the stability characteristics. Experimental measurements of shear flows have provided the basis for simple analytical forms to describe the mean flow in the stability calculations. Such mean flow data are lacking for two stream coaxial jets, especially at supersonic conditions. The data that are available are not sufficient to develop analytical expressions for the mean flow properties of coaxial jets that transition smoothly from two streams to one fully developed jet downstream for both normal velocity profile and inverted velocity profile cases. A numerical scheme has been developed to calculate the mean flow properties of a coaxial jet with two initial shear layers. The development of a turbulent, axisymmetric free jet is assumed to be governed by the Reynolds-averaged, compressible, parabolic boundary layer equations. To complete this set of equations, a turbulence model is necessary. Any turbulence model chosen for these calculations would have required modification and calibration to obtain reasonable results for both normal and inverted profile coaxial jets. For expediency, a modified and calibrated mixing length model has been used to represent the turbulent stresses and obtain an effective viscosity. Mean flow properties have been predicted for coaxial jets with either a normal initial velocity profile or an inverted initial velocity profile that expand and merge in a manner representative of measured data. Both good qualitative and quantitative agreement has been found for both velocity and temperature profiles. These mean flow results can be used to calculate instability wave characteristics for coaxial jets. These calculations are described in subsequent papers for both NVP [4] and IVP [5] jets.

REFERENCES

1. J. M. Seiner and E. A. Krejsa 1989 *AIAA Paper No*. 89-2358. Supersonic jet noise and the high speed civil transport.
2. H. K. Tanna 1977 *Journal of Sound and Vibration* **50**, 429–444. An experimental study of jet noise, part II: shock associated noise.
3. H. K. Tanna, W. H. Brown and C. K. W. Tam 1981 *NASA CR*-3454. Shock associated noise reduction from inverted-velocity-profile coannular jets.
4. M. D. Dahl and P. J. Morris 1997 *Journal of Sound and Vibration* **200**, 665–699. Noise from supersonic coaxial jets, part 2: normal velocity profile.
5. M. D. Dahl and P. J. Morris 1997 *Journal of Sound and Vibration* **200**, 701–719. Noise from supersonic coaxial jets, part 3: inverted velocity profile.
6. J. C. Lau, P. J. Morris and M. J. Fisher 1979 *Journal of Fluid Mechanics* **93**, 1–27. Measurements in subsonic and supersonic free jets using a laser velocimeter.
7. J. Cohen and I. Wygnanski 1987 *Journal of Fluid Mechanics* **176**, 191–219. The evolution of instabilities in the axisymmetric jet, part 1: the linear growth of disturbances near the nozzle.
8. G. L. Morrison and D. K. McLaughlin 1980 *American Institute of Aeronautics and Astronautics Journal* **18**, 793–800. Instability process in low Reynolds number supersonic jets.
9. A. Michalke 1984 *Progress in Aerospace Sciences* **21**, 159–199. Survey of jet instability theory.
10. H. Schlichting 1979 *Boundary-layer Theory*. New York: McGraw-Hill; seventh edition.
11. F. M. White 1974 *Viscous Fluid Flow*. New York: McGraw-Hill.
12. M. D. Dahl 1994 *Ph.D. dissertation*, *Penn State University*. The aeroacoustics of supersonic coaxial jets.

13. C. K. W. Tam and P. J. Morris 1990 *Journal of Fluid Mechanics* **98**, 349–381. The radiation of sound by the instability waves of a compressible plane turbulent shear layer.
14. C. K. W. Tam and D. E. Burton 1984 *Journal of Fluid Mechanics* **138**, 273–295. Sound generated by instability waves of supersonic flows, part 2: axisymmetric jets.
15. P. J. Morris 1980 *AIAA Paper No*. 80-1004. A model for broadband jet noise amplification.
16. P. J. Morris and C. Baltas 1981 *AIAA Paper No*. 81-0058. Turbulence in sound excited jets: measurements and theory.
17. C. Y. Chen 1976 *AIAA Paper No*. 76-4. A model for predicting aero-acoustic characteristics of coaxial jets.
18. T. F. Balsa and P. R. Gliebe 1977 *American Institute of Aeronautics and Astronautics Journal* **15**, 1550–1558. Aerodynamics and noise of coaxial jets.
19. P. R. Gliebe and T. F. Balsa 1978 *Journal of Aircraft* **15**, 743–749. Aeroacoustics of axisymmetric single- and dual-flow exhaust nozzles.
20. N. J. Georgiadis and D. A. Yoder 1994 *AIAA Paper No*. 94-3212. Use of Navier–Stokes methods for the calculation of high-speed nozzle flow fields.
21. S. V. Patankar and D. B. Spalding 1970 *Heat and Mass Transfer in Boundary Layers*. London: Intertext; second edition.
22. D. A. Anderson, J. C. Tannehill and R. H. Pletcher 1984 *Computational Fluid Mechanics and Heat Transfer*. New York: Hemisphere.
23. P. Bradshaw 1977 *Annual Review of Fluid Mechanics* **9**, 33–54. Compressible turbulent shear layers.
24. S. M. Dash, N. Sinha and D. C. Kenzakowski 1992 *DGLR/AIAA Paper No*. 92-02-106. The critical role of turbulence modeling in the prediction of supersonic jet structure for acoustic applications.
25. NASA 1972 *Free Turbulent Shear Flows*. SP-321.
26. M. E. Crawford and W. M. Kays 1976 *NASA CR*-2742. Stan5—a program for numerical computation of two-dimensional internal and external boundary layer flows.
27. G. L. Brown and A. Roshko 1974 *Journal of Fluid Mechanics* **64**, 775–816. On density effects and large structure in turbulent mixing layers.
28. D. Papamoschou and A. Roshko 1988 *Journal of Fluid Mechanics* **197**, 453–477. The compressible turbulent shear layer: an experimental study.
29. P. J. Morris 1976 *AIAA Paper No*. 76-25. Turbulence measurements in subsonic and supersonic axisymmetric jets in a moving stream.
30. J. C. Lau 1980 *Lockheed-Georgia Co*. LG80ER0017. A study of the structure of the coannular jet.
31. I. K. Madni and R. H. Pletcher 1975 *Journal of Fluids Engineering* **97**, 558–567. Prediction of turbulent jets in coflowing and quiescent ambients.
32. L. F. Donovan and C. A. Todd 1967 *NASA TN D*-4378. Computer program for calculating isothermal, turbulent jet mixing of two gases.
33. K. B. M. Q. Zaman 1986 *Journal of Sound and Vibration* **106**, 1–16. Flow field and near and far sound field of a subsonic jet.
34. P. O. Witze 1974 *American Institute of Aeronautics and Astronautics Journal* **12**, 417–418. Centerline velocity decay of compressible free jets.
35. J. C. Lau 1981 *Journal of Fluid Mechanics* **105**, 193–218. Effects of exit mach number and temperature on mean-flow and turbulence characteristics in round jets.
36. J. M. Eggers 1966 *NASA TN D*-3601. Velocity profiles and eddy viscosity distributions downstream of a Mach 2.22 nozzle exhausting to quiescent air.
37. U. von Glahn, J. Goodykoontz and C. Wasserbauer 1986 *AIAA Paper No*. 86-0312. Velocity and temperature decay characteristics of inverted-profile jets.
38. H. K. Tanna, B. J. Tester and J. C. Lau 1979 *NASA CR*-158995. The noise and flow characteristics of inverted-profile coannular jets.
39. P. E. Dimotakis 1986 *American Institute of Aeronautics and Astronautics Journal* **24**, 1791–1796. Two-dimensional shear-layer entrainment.
40. N. L. Messersmith, S. G. Goebel, W. H. Frantz, E. A. Krammer, J. P. Renie, J. C. Dutton and H. Krier 1988 *AIAA Paper No*. 88-0702. Experimental and analytical investigations of supersonic mixing layers.
41. P. E. Dimotakis 1989 *AIAA Paper No*. 89-0262. Turbulent free shear layer mixing.
42. G. A. Sullins 1989 *NASP CR* 1053. Shear layer mixing tests.
43. S. G. Goebel and J. C. Dutton 1991 *American Institute of Aeronautics and Astronautics Journal* **29**, 538–546. Experimental study of compressible turbulent mixing layers.

APPENDIX A: CALIBRATION OF THE MIXING LENGTH MODEL

A.1. INCOMPRESSIBLE FACTOR C_1

For given flow conditions, the mixing length model must provide the effective viscosity that causes the jet shear layer to spread. C_1 is the only factor available for adjustment in order to obtain the proper spreading rate when the flow is incompressible. Many authors have used experimental evidence and arguments about large scale structures dominating the development of turbulent shear layers (some recent references are references [28] and [39–43]) to develop a prediction for the incompressible vorticity thickness growth rate δ_ω/x as a function of the velocity ratio r and the density ratio s,

$$\frac{\delta_\omega}{x} = 0{\cdot}088\,\frac{|1-r|(1+\sqrt{s})}{1+r\sqrt{s}}, \tag{A1}$$

where $r = U_2/U_1$ and $s = \rho_2/\rho_1$. The constant 0·088 used here is an average of the constants from the above references when all are converted to a vorticity thickness growth rate, either from information given in the reference or from the assumption of an error function shape for the velocity profile. Although equation (A1) has been developed for a planar shear layer, it is assumed to hold in the initial core region of a jet where there is a constant velocity at both edges of the shear layer.

The calibration of C_1 is carried out for a range of expected r and s values. Given r and s, C_1 is varied until the calculated vorticity thickness growth rate in the core region agrees with that predicted by equation (A1). To ensure that μ_T dominates the effective viscosity and that the flow is essentially incompressible, the calculations have been carried out on a low speed, large diameter jet such that the Reynolds number was greater than 10^6 and $\mu_T \gg \mu$. The resulting family of curves is correlated to develop an equation for C_1 for $r < 1$ and an equation for $r > 1$. The curves take the form

$$C_1(r,s) = \frac{A(r) + B(r)\sqrt{s} + C(r)s}{(1+\sqrt{s})(1+r\sqrt{s})}, \tag{A2}$$

where, for $r < 1$,

$$A(r) = (6{\cdot}5919 + 11{\cdot}918r - 4{\cdot}1855r^2) \times 10^{-2},$$

$$B(r) = (10{\cdot}880 - 2{\cdot}3578r + 6{\cdot}5642r^2) \times 10^{-2},$$

$$C(r) = (3{\cdot}1013 + 16{\cdot}420r - 5{\cdot}8217r^2) \times 10^{-2}$$

and, for $r > 1$,

$$A(r) = (101{\cdot}95 + 51{\cdot}507r - 1{\cdot}6000r^2) \times 10^{-3},$$

$$B(r) = (60{\cdot}287 + 75{\cdot}160r + 1{\cdot}3818r^2) \times 10^{-3},$$

$$C(r) = (723{\cdot}97 + 753{\cdot}34r - 6{\cdot}2101r^2) \times 10^{-4}.$$

A.2. COMPRESSIBILITY FACTOR C_2

To develop the compressibility factor, experimental results for compressible shear layers have been used to make a plot of normalized vorticity thickness growth rates versus convective Mach number [12]. A simple curve fit to this data is given by

$$\delta'_\omega(M_c)/\delta'_{\omega o} = 1 + 0{\cdot}785[\exp(-2M_c^2) - 1], \tag{A3}$$

where the convective Mach number is

$$M_c = M_1 \frac{\sqrt{s}|1 - r|}{1 + \sqrt{s}}, \tag{A4}$$

$\delta'_{\omega o}$ is the incompressible spreading rate for the same r and s, and M_1 is the Mach number for the stream with velocity U_1.

For given r, s and M_1, C_2 is adjusted, allowing C_1 to take on its value defined by equation (A2), until the calculated compressible vorticity thickness growth rate in the core region agrees with the value predicted by equation (A3), when $\delta'_{\omega o}$ is given by equation (A1). The results for C_2 have been correlated with M_c to obtain the following equation:

$$C_2(M_c) = 1 + 0{\cdot}4959[\exp(-1{\cdot}4593M_c^2 + 0{\cdot}0427M_c^2 - 0{\cdot}3658M_c^4) - 1]. \tag{A5}$$